Amin Soltani, An Deng, Abbas Taheri, Asuri Sridharan and A.R. Estabragh
A framework for interpretation of the compressibility behavior of soils
Geotechnical Testing Journal, 2018; 41(1):1-16

Originally published at http://dx.doi.org/10.1520/GTJ20170088

Geotechnical Testing Journal

doi:10.1520/GTJ20170088 / Vol. 41 / No. 1 / January 2018 / available online at www.astm.org

Amin Soltani,[1] An Deng,[2] Abbas Taheri,[2] Asuri Sridharan,[3,4] and A. R. Estabragh[5]

A Framework for Interpretation of the Compressibility Behavior of Soils

Reference

Soltani, A., Deng, A., Taheri, A., Sridharan, A., and Estabragh, A. R., "A Framework for Interpretation of the Compressibility Behavior of Soils," *Geotechnical Testing Journal*, Vol. 41, No. 1, 2018, pp. 1–16, https://doi.org/10.1520/GTJ20170088. ISSN 0149-6115

ABSTRACT

This paper aims at the development of a regression-aided analytical framework for modeling and analyzing the compressibility behavior of over-consolidated soils. A three-parameter rectangular hyperbola function (3P-RH) was proposed for describing the void ratio–effective stress relationship. Validation of the 3P-RH was carried out by a compiled database gathered from the literature. Simple analytical solutions were then proposed for determining the compressibility curve variables including the compression (C_c) and recompression (C_r) indices and the preconsolidation pressure (P_c), which are intended to replace the current subjective graphical method by providing consistent results. Equations for the preconsolidation pressure were derived in accordance with four common graphical constructions covering various levels of geometrical complexity (slightly to highly subjective). A probabilistic comparison among the graphical constructions was then carried out. Furthermore, a sensitivity analysis with respect to the proposed preconsolidation pressure functions was considered to evaluate the influence of the 3P-RH fitting parameters (α and β) on the preconsolidation pressure value. The proposed 3P-RH compressibility model accompanied by the suggested analytical solutions for solving the compressibility curve variables construct a unique framework for modeling the compressibility behavior of soils with an acceptable degree of accuracy and, more importantly, by a simple objective approach.

Keywords

regression-aided analytical framework, compressibility, three-parameter rectangular hyperbola, compression index, recompression index, preconsolidation pressure

Manuscript received March 18, 2017; accepted for publication July 6, 2017; published online December 7, 2017.

[1] School of Civil, Environmental and Mining Engineering, The University of Adelaide, Adelaide, SA 5005, Australia (Corresponding author), e-mail: amin.soltani@adelaide.edu.au, https://orcid.org/0000-0002-0483-7487

[2] School of Civil, Environmental and Mining Engineering, The University of Adelaide, Adelaide, SA 5005, Australia

[3] Department of Civil Engineering, Indian Institute of Science, Bangalore 560012, India

[4] Indian National Science Academy, New Delhi 110009, India

[5] Faculty of Soil and Water Engineering, University of Tehran, PO BOX 4411, Karaj 31587-77871, Iran, https://orcid.org/0000-0003-4545-2310

Nomenclature

e = void ratio
σ' = vertical effective stress
C_c = compression index (e:logσ' space)
C_r = recompression index (e:logσ' space)

λ = compression index (e:lnσ' space)
κ = recompression index (e:lnσ' space)
C_c' = compression index (log$e$:logσ' space)
C_r' = recompression index (log$e$:logσ' space)
P_c = preconsolidation pressure
PCL = vertical preconsolidation pressure line
VCL = virgin compression line (e:logσ' space)
RCL = recompression line (e:logσ' space)
$\overline{\text{VCL}}$ = virgin compression line (log$e$:logσ' space)
$\overline{\text{RCL}}$ = recompression line (log$e$:logσ' space)
3P-RH = three-parameter rectangular hyperbola function
e_0 = initial void ratio
α = fitting parameter of the 3P-RH
β = fitting parameter of the 3P-RH
f' = first derivative of the 3P-RH (e:logσ' space)
f'' = second derivative of the 3P-RH (e:logσ' space)
f''' = third derivative of the 3P-RH (e:logσ' space)
$f'_{\log}$ = first derivative of the 3P-RH (log$e$:logσ' space)
$f''_{\log}$ = second derivative of the 3P-RH (log$e$:logσ' space)
MTL = tangent thorough the maximum curvature point
HML = horizontal line through the maximum curvature point
BSL = bisector line
IVL = horizontal initial void ratio line
θ = acute angle formed between MTL and HML
S_M = slope of MTL
S_B = slope of BSL
P_c^{M1} = preconsolidation pressure with respect to the Classical method
P_c^{M1S} = preconsolidation pressure with respect to the Simplified Classical method
P_c^{M2} = preconsolidation pressure with respect to the Silva method
P_c^{M3} = preconsolidation pressure with respect to the RCL-VCL Intercept method
P_c^{M4} = preconsolidation pressure with respect to the Log-Log method
$NRMSE$ = normalized root mean square error
x_i = independent variable
S_{x_i} = sensitivity to variations in x_i
$\mu_{x_i}^+$ = positive magnitude caused by increase in x_i
$\mu_{x_i}^-$ = negative magnitude cause by increase in x_i

Introduction

The compressibility behavior of soils is often studied by means of the conventional oedometer test. As a result of the test, a change in void ratio against the corresponding effective stress can be observed. The void ratio–effective stress relationship, commonly illustrated over a semi-log space (e:logσ'), contains fundamental information required for settlement analysis. Several researchers (Butterfield 1979; Cargill 1984; Burland 1990; Houlsby and Wroth 1991; Pestana and Whittle 1995; McNabb and Boersma 1996; Arvidsson and Keller 2004; Baumgartl and Köck 2004; Gregory et al. 2006; Liu, Xu, and Horpibulsuk 2012; Chong and Santamarina 2016) have proposed various forms of mathematically defined compressibility models to describe the void ratio–effective stress relationship. Generally, any introduced model is expected to be valid over a wide range of soils, have physically correct boundary values corresponding to low ($\sigma'\to 0^+$) and high ($\sigma'\to+\infty$) stress states, and, most importantly, involve physically meaningful parameters (Chong and Santamarina 2016; Soltani 2016). In addition to these fundamental criteria, the model should represent the most simple yet accurate functional form possible. This basically implies that any proposed compressibility function, say $f(x)$, should provide simple explicit solutions to $f(x)=0$, $f'(x)=0$, $f''(x)=0$, and $f'''(x)=0$ over the e:logσ' space. This particular feature assumes significance when trying to mathematically solve the compressibility curve variables, including the compression (C_c) and recompression (C_r) indices and the yield effective stress, better known as the preconsolidation pressure (P_c). The majority of available models, however, fail to satisfy some of these fundamentals and, therefore, lack the required versatility of being promoted as a universal function for the purpose of numerical applications. The hyperbolic function has been widely credited as a useful mathematical concept for describing a multitude of physical phenomena in geotechnical engineering. Different forms of the hyperbolic relationship have been suggested and successfully tested for describing various geotechnical-related problems such as stress-strain behavior of soils (Duncan and Chang 1970; Boscardin et al. 1990; Stark, Ebeling, and Vettel 1994; Sridharan and Gurtug 2005) and the strain-time relationship of compressible and swelling soils (Sridharan and Sreepada Rao 1981; Sridharan, Rao, and Sivapullaiah 1986a; Sivapullaiah, Sridharan, and Stalin 1996; Sridharan and Gurtug 2004; Al-Shamrani 2005). A literature survey, however, indicates that various aspects of the hyperbolic function have not yet been fully evaluated in describing the compressibility curve variables. In this study, a three-parameter rectangular hyperbola (3P-RH) was adopted and validated for modeling the void ratio–effective stress relationship, which can be given as:

$$e(\sigma') = e_0 - \frac{\sigma'}{\alpha+\beta\sigma'}$$
$$\text{Boundary conditions}: \begin{cases} e(0) = e_0 \\ \lim\limits_{\sigma'\to+\infty}[e(\sigma')] \cong e_0 - \frac{1}{\beta} \end{cases} \quad (1)$$

where:

$e(\sigma')$ = void ratio with respect to effective stress σ',
e_0 = initial void ratio, and
α and β = fitting parameters, α in kPa.

Fig. 1 illustrates the general form of a typical 3P-RH function, specified as f, accompanied by its first, second, and third derivatives (f', f'', and f''') with respect to the e:logσ' space over

FIG. 1 Illustration of a typical 3P-RH function (Eq 1) accompanied by its first, second, and third derivatives with respect to the *e*:logσ' space.

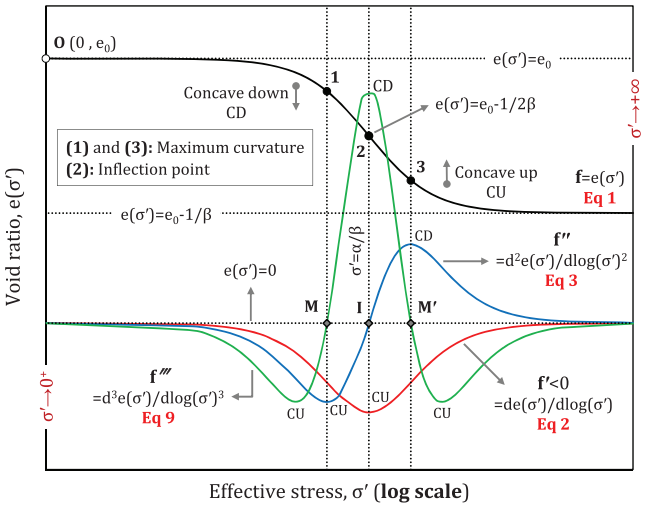

$\sigma' \in (0,+\infty)$. The 3P-RH poses as a reversed *S*-shaped curve, which corresponds to the positive asymptotic values of e_0 and e_0-$1/\beta$ at low ($\sigma' \to 0^+$) and high ($\sigma' \to +\infty$) stress states, respectively. All three derivatives correspond to the asymptotic value of zero at $\sigma' \to 0^+$ and $\sigma' \to +\infty$. f' poses as a *U*-shaped curve and thus assumes a negative value over the entire effective stress domain ($f' < 0$), basically resembling the decreasing trend of e as a result of increase in σ'. f'', however, demonstrates a fall-rise-fall behavior containing two global extrema points, a minimum and a maximum. $f'' = 0$ has one real root (point I in **Fig. 1**), which is defined as the global minimum of f' and, more importantly, the inflection point of the 3P-RH (point 2). f''' graphically corresponds to two equal global minimums and a global maximum. $f''' = 0$ has two real roots (points M and M′), representing the global minimum and maximum of f'' and, more importantly, points with maximum curvature on the 3P-RH (points 1 and 3).

Fig. 2 illustrates the general form of the compressibility curve with respect to the 3P-RH model for a typical over-consolidated soil over the *e*:logσ' space. The curve can be generally divided into two regions, namely the elastic and plastic compression zones, which are phases in which the compression process takes place. The two regions are separated by the preconsolidation pressure (PCL in **Fig. 2**), a transitional stress state that divides the soil's compressibility into a region of small-elastic (recompression stage) and large-plastic (virgin compression stage) deformations (Casagrande 1936; Dias Junior and Pierce 1995; Boone 2010). The compressibility curve variables C_c, C_r, and P_c are normally determined by a conventional graphical procedure. For this purpose, a tangent, defined as the virgin compression line (VCL), is drawn through the inflection point of the compressibility curve. An additional tangent, the recompression line (RCL), is then extended through point A (initial loading stage). Slope of the VCL and RCL are then obtained and defined as C_c and C_r, respectively. The preconsolidation pressure, however, remains a rather ambiguous concept. A number of methods have been proposed for the interpretation of this parameter, which will be outlined during the course of this paper. The majority of these methods are basically graphical approaches that are highly subjective and thus promote inconsistent results among individuals. The

FIG. 2 Interpretation of the preconsolidation pressure with respect to the 3P-RH compressibility model by means of the "Classical" graphical construction or M1/M1S (Eq 15 or 17).

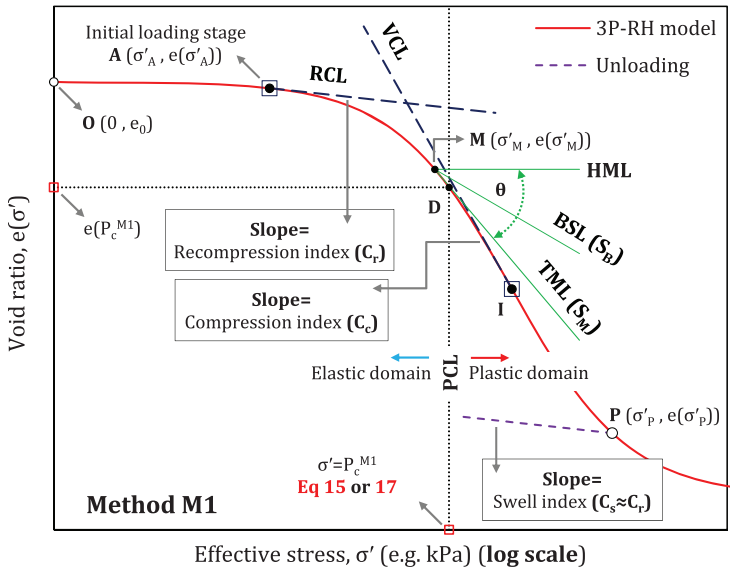

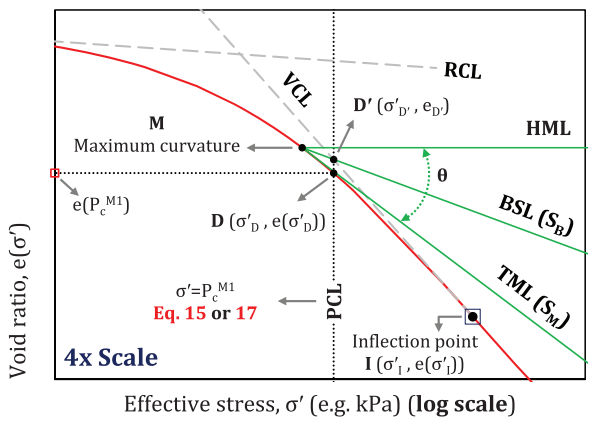

preconsolidation pressure has been widely credited as an extraordinarily useful concept for analyzing and predicting settlement behavior, normalizing other geotechnical engineering parameters for comparative purposes and advancing constitutive modeling (Ladd and Foott 1974; Boone 2010).

An accurate estimation of the compressibility curve variables is essential for the calculation of primary consolidation settlement, which plays a key role in the design of cost-effective foundation systems. The current graphical concept for determining these variables, particularly the preconsolidation pressure, is strongly associated with subjective judgements and a high degree of uncertainty, not to mention being problematic and time consuming when being applied over a semilog plot (Becker et al. 1987; Dias Junior and Pierce 1995; Grozic, Lunne, and Pande 2003; Baumgartl and Köck 2004; Boone 2010). In this paper, an attempt has been made to derive simple equations by means of a regression-aided analytical concept for determining these variables. The presence of such relationships intends to aid computational analyses and can replace the conventional graphical construction by providing consistent results.

Proposed Framework

COMPRESSION AND RECOMPRESSION INDICES

The inflection point resembles a state within the plastic compression region, which best represents an ideal linear behavior. A necessary condition for $x \in D_{f(x)}$ (domain function) to be defined as the inflection point of $f(x)$ is that the second derivative over the $f(x)$:log$x$ space should be equal to zero. Therefore, the inflection point of the 3P-RH compressibility function or Eq 1 (point I in **Fig. 2**) can be obtained by the following three-step procedure:

$$f' = \frac{de(\sigma')}{d\log\sigma'} = \frac{\partial e(\sigma')}{\partial \sigma'} \times \sigma' \times \ln 10 = \frac{-\ln 10 \alpha \sigma'}{(\alpha + \beta\sigma')^2} \tag{2}$$

$$f'' = \frac{df'}{d\log\sigma'} = \frac{\partial f'}{\partial \sigma'} \times \sigma' \times \ln 10 = \frac{-(\ln 10)^2 \alpha\sigma'(\alpha - \beta\sigma')}{(\alpha + \beta\sigma')^3} \tag{3}$$

$$f'' = 0 : \begin{cases} \sigma'_I = \frac{\alpha}{\beta} \\ e(\sigma'_I) = e_0 - \frac{1}{2\beta} \end{cases} \tag{4}$$

Slope of the tangent to the compressibility curve at the inflection point (VCL in **Fig. 2**), defined as C_c, can now be obtained by substituting the inflection point value (Eq 4) into f' (Eq 2), which results in the following:

$$C_c = \left.\frac{de(\sigma')}{d\log\sigma'}\right|_{\sigma' = \frac{\alpha}{\beta}} = \frac{-\ln 10}{4\beta} \tag{5}$$

C_r, equivalent to the swell index (C_s in **Fig. 2**), is defined as slope of the RCL. Therefore, by calculating f' (Eq 5) at $\sigma' = \sigma'_A$ (initial effective stress applied in a typical compression test, which is basically user defined), the following can be obtained for C_r:

$$C_r = \left.\frac{de(\sigma')}{d\log\sigma'}\right|_{\sigma' = \sigma'_A} = \frac{-\ln 10 \alpha \sigma'_A}{(\alpha + \beta\sigma'_A)^2} \tag{6}$$

In conjunction with the critical state theory, C_c and C_r are defined over the e:lnσ' space and are commonly referred to as λ and κ, respectively. Applying the basic logarithmic law $\ln x = \ln 10 \times \log x$, one can obtain the following for λ and κ:

$$\lambda = \frac{C_c}{\ln 10} = \frac{-1}{4\beta} \tag{7}$$

$$\kappa = \frac{C_r}{\ln 10} = \frac{-\alpha\sigma'_A}{(\alpha + \beta\sigma'_A)^2} \tag{8}$$

As Eqs 5 to 8 represent the slope of lines with a decreasing trend, they generate negative values. In conjunction with settlement computations, however, the absolute value of these equations should be considered.

PRECONSOLIDATION PRESSURE

Numerous methods have been proposed by several researchers (Casagrande 1936; Janbu 1969; Pacheco Silva 1970; Butterfield 1979; Becker et al. 1987; Oikawa 1987; Jose, Sridharan, and Abraham 1989; Burland 1990; Sridharan, Abraham, and Jose 1991; Onitsuka et al. 1995; Cui and Delage 1996; Grozic, Lunne, and Pande 2003; Boone 2010; Ku and Mayne 2013) for the interpretation of the preconsolidation pressure by means of standard oedometeric test data. The majority of these methods are generally graphical constructions defined in the space of e:logσ' or log$e$:logσ', most of which seem to be founded based on similar empirical observations with respect to e-σ' stress patterns exhibited by different soils (a detailed discussion may be found in Boone [2010]). In this paper, overlooking the possible advantages a particular approach may pose over another, four most commonly adopted techniques, covering various levels of geometrical complexity, were investigated. The objective was to demonstrate how various graphical scenarios ranking from basic (slightly subjective) to complex (highly subjective) may be mathematically formulized. Generally, the proposed analytical concept should be applicable to other compressibility functions and any graphical construction that defines P_c in the space of e:logσ' or log$e$:logσ'. The presence of mathematically defined relationships for P_c that promote a nonsubjective framework may also well provide a realistic basis for comparing the available graphical approaches in this context.

The Classical Method

The Casagrande (1936) approach, recognized as the Classical method (herein M1), is the oldest and probably the most commonly adopted technique for determining the preconsolidation pressure. The method follows a relatively complex graphical procedure, which has been outlined in **Fig. 2**. For this purpose, a tangent (MTL) is drawn through the maximum curvature point M.

A horizontal line, specified as HML, is then extended from point M to form an acute angle (θ) with MTL. A bisector with respect to θ (BSL) is then graphically produced and extended to meet the VCL at point D′, which is defined as the preconsolidation pressure. The crux of this graphical construction is defining the maximum curvature point, a highly subjective task, indeed. Defining a point with maximum curvature using a semilog plot is highly associated with personal judgement, yielding nonconsistent results by different users. Furthermore, defining the point M is known to become an increasingly difficult task in the case of sample disturbance (Janbu 1969; Sridharan, Abraham, and Jose 1991; Dias Junior and Pierce 1995; Grozic, Lunne, and Pande 2003; Boone 2010). The method has also proven to be highly influenced by the scaling effect, an inseparable quirk associated with plotting (Sridharan, Abraham, and Jose 1991; Clementino 2005; Boone 2010). Good results may be obtained, providing that the break point (point D) is subjectively well defined.

The second derivative of $f(x)$ is known to measure the degree of curvature or concavity. A necessary condition for $x \in D_{f(x)}$ to be defined as an absolute maximum curvature point is that the third derivative of the 3P-RH over the $f(x)$:log$x$ space should be equal to zero (Baumgartl and Köck 2004; Imhoff, Da Silva, and Fallow 2004; Gregory et al. 2006). This is basically analogous to maximizing the second derivative f'' (Eq 3), which can be given by the following procedure:

$$f''' = \frac{\mathrm{d}f''}{\mathrm{d}\log\sigma'} = \frac{\partial f''}{\partial \sigma'} \times \sigma' \times \ln 10 = \frac{-(\ln 10)^3 \alpha\sigma'(\alpha^2 - 4\alpha\beta\sigma' + \beta^2\sigma'^2)}{(\alpha + \beta\sigma')^4} \tag{9}$$

$$f''' = 0 : \begin{cases} \sigma'_{\mathrm{M}} = \frac{1}{2+\sqrt{3}}\left(\frac{\alpha}{\beta}\right) \approx 0.268\left(\frac{\alpha}{\beta}\right) \\ e(\sigma'_{\mathrm{M}}) = e_0 - \frac{2}{3+\sqrt{3}}\left(\frac{1}{2\beta}\right) \approx e_0 - 0.423\left(\frac{1}{2\beta}\right) \end{cases} \tag{10}$$

Slope of MTL (S_{M} in **Fig. 2**) can be obtained by substituting the maximum curvature point value (Eq 10) into the first derivative f' (Eq 2), which results in the following:

$$S_{\mathrm{M}} = -\tan\theta = \left.\frac{\mathrm{d}e(\sigma')}{\mathrm{d}\log\sigma'}\right|_{\sigma' = \sigma'_{\mathrm{M}}} = \frac{-\ln 10}{6\beta} \tag{11}$$

Considering basic geometrical principles, slope of BSL or S_{B} can be expressed as:

$$S_{\mathrm{B}} = -\tan\frac{\theta}{2} = \tan\left[\frac{1}{2}\tan^{-1}\overbrace{\left(\frac{-\ln 10}{6\beta}\right)}^{S_{\mathrm{M}}}\right] = \frac{\sqrt{1+S_{\mathrm{M}}^2}-1}{S_{\mathrm{M}}} \tag{12}$$

Considering basic geometrical relationships between C_c (slope of the VCL determined by Eq 5) and the inflection point I (a point on the VCL given by Eq 4), the VCL can be expressed by the following linear relationship in the e:logσ' space:

$$\mathrm{VCL}: e = \overbrace{\frac{-\ln 10}{4\beta}}^{C_c} \times \log\left(\frac{\beta}{\alpha}\sigma'\right) + \overbrace{e_0 - \frac{1}{2\beta}}^{e(\sigma'_1)} \tag{13}$$

Similarly, the BSL can be represented by means of S_{B} (Eq 12) and the maximum curvature point M (Eq 10) as the following:

$$\mathrm{BSL}: e = \overbrace{\frac{\sqrt{1+S_{\mathrm{M}}^2}-1}{S_{\mathrm{M}}}}^{S_{\mathrm{B}}} \times \log\left[\frac{(2+\sqrt{3})\beta}{\alpha}\sigma'\right] + \overbrace{e_0 - \frac{2}{3+\sqrt{3}}\left(\frac{1}{2\beta}\right)}^{e(\sigma'_{\mathrm{M}})} \tag{14}$$

Intersection of the VCL and BSL (point D′ in **Fig. 2**), defined as the M1 preconsolidation pressure (P_c^{M1}), can now be obtained by equating Eqs 13 and 14, which yields the following:

$$\sigma'_{\mathrm{D}'} = \sigma'_{\mathrm{D}} = P_c^{\mathrm{M1}} = 10^{\frac{C_c \log\left(\frac{\alpha}{\beta}\right) - S_{\mathrm{B}} \log\left[\frac{1}{2+\sqrt{3}}\left(\frac{\alpha}{\beta}\right)\right] + \frac{\sqrt{3}}{6\beta}}{C_c - S_{\mathrm{B}}}} \tag{15}$$

The void ratio at points D′ and D can also be obtained by substituting $\sigma' = P_c^{\mathrm{M1}}$ (Eq 15) into the VCL linear relationship (Eq 13) and the 3P-RH (Eq 1), respectively.

Assuming $\theta \approx \tan\theta$, an alternate relationship of much greater flexibility compared to Eq 12 can be obtained for S_{B}. While the simplification should slightly overestimate S_{B}, it will later be proven to generate acceptable results for a wide range of scenarios. The simplification promotes the following alternate relationship for S_{B}:

$$S_{\mathrm{B}} \approx \frac{S_{\mathrm{M}}}{2} = \frac{-\ln 10}{12\beta} \tag{16}$$

Considering the recent Eq 16, a simplified alternative to P_c^{M1} (Eq 15), termed as P_c^{M1S}, can be derived as:

$$P_c^{\mathrm{M1S}} = 10^{\frac{3}{2}\log\left(\frac{\alpha}{\beta}\right) - \frac{1}{2}\log\left[\frac{1}{2+\sqrt{3}}\left(\frac{\alpha}{\beta}\right)\right] - \frac{\sqrt{3}}{\ln 10}} = \frac{\dot{e}^{-\sqrt{3}}}{\sqrt{2-\sqrt{3}}}\left(\frac{\alpha}{\beta}\right) \approx 0.342\left(\frac{\alpha}{\beta}\right) \tag{17}$$

where:

$\dot{e}$ = Euler's number, $\dot{e} \approx 2.718$.

The Silva Method

The graphical procedure of determining the preconsolidation pressure as proposed by Pacheco Silva (1970), recognized as the Silva construction (herein M2), is illustrated in **Fig. 3**. The Silva approach for defining P_c involves following the respective path of B′→B→S′→S. For this purpose, the horizontal initial void ratio line $e(\sigma') = e_0$ (IVL) is drawn over the entire effective stress domain. The VCL is then extended to a point at which it intersects the IVL at point B′. A vertical line is then extended downward from point B′, which meets the compressibility curve at

point B. Finally, point B is extended horizontally in order to meet the VCL at point S′, which is defined as the preconsolidation pressure. The method strongly relies on an accurate interpretation of the VCL. Boone (2010) demonstrated a subjective variability of nearly 65 % with respect to the Silva approach using two different yet common interpretations of the VCL. However, the method has been widely credited as being independent of the drawing scale (Clementino 2005; Boone 2010).

The intersection of the IVL and VCL (point B′ in **Fig. 3**) can be obtained by equating the VCL (Eq 13) to e_0. In this case, the following can be derived for $\sigma'_{B'}$:

$$\sigma'_{B'} = \sigma'_B = 10^{\log\left(\frac{\alpha}{\beta}\right)-\frac{2}{\ln 10}} = \frac{1}{\dot{e}^2}\left(\frac{\alpha}{\beta}\right) \approx 0.368\left(\frac{\alpha}{\beta}\right) \tag{18}$$

The void ratio at point B can be determined by calculating the value of the 3P-RH (Eq 1) at $\sigma' = \sigma'_{B'} = \sigma'_B$ (Eq 18), which results in the following:

$$e(\sigma'_B) = e_0 - \frac{2}{\dot{e}^2+1}\left(\frac{1}{2\beta}\right) \approx e_0 - 0.238\left(\frac{1}{2\beta}\right) \tag{19}$$

Point S′ on the VCL has an equal void ratio value to that of point B; therefore, by equating Eqs 13 and 19, the following can be derived for obtaining the effective stress at point S′, which also represents the M2 preconsolidation pressure (P_c^{M2}):

$$\sigma'_{S'} = \sigma'_S = P_c^{M2} = 10^{\log\left(\frac{\alpha}{\beta}\right)-\frac{2}{\ln 10}\left(\frac{\dot{e}^2-1}{\dot{e}^2+1}\right)} = \dot{e}^{-2\left(\frac{\dot{e}^2-1}{\dot{e}^2+1}\right)}\left(\frac{\alpha}{\beta}\right) \approx 0.218\left(\frac{\alpha}{\beta}\right) \tag{20}$$

The void ratio corresponding to P_c^{M2} on the 3P-RH ($e(P_c^{M2})$) can be further obtained substituting $\sigma' = P_c^{M2}$ (Eq 20) in Eq 1.

The RCL-VCL Intercept Method

Fig. 4 shows the graphical construction in accordance with the RCL-VCL Intercept approach, herein M3, for determining the preconsolidation pressure. As the name of the method implies, the M3 preconsolidation pressure (P_c^{M3}) is defined as the intersection of the RCL and VCL (point C′ in **Fig. 4**). The method probably proposes the least subjective approach among others that only rely on an accurate interpretation of the RCL and VCL. The approach seems to be a common practice among researchers (Cui and Delage 1996; Alonso et al. 2005; Gregory et al. 2006; Estabragh, Bordbar, and Javadi 2011; Estabragh and Javadi 2013; Estabragh et al. 2014). However, applying the technique over a semilog plot may still be associated with some difficulties, not to mention being inconvenient for numerical implementations.

The M3 preconsolidation pressure can be obtained by equating the VCL (Eq 13) and RCL linear relationships. Considering basic geometrical relationships between C_r (Eq 6) and the user-defined point A, the RCL can be expressed as the following:

$$\text{RCL}: e = \overbrace{\frac{-\ln 10\alpha\sigma'_A}{(\alpha+\beta\sigma'_A)^2}}^{C_r} \times \log\left(\frac{\sigma'}{\sigma'_A}\right) + \overbrace{e_0 - \frac{\sigma'_A}{\alpha+\beta\sigma'_A}}^{e(\sigma'_A)} \tag{21}$$

By equating Eqs 13 and 21 and rearranging, the following can be obtained for solving point C′, hence obtaining P_c^{M3}:

$$\sigma'_{C'} = \sigma'_C = P_c^{M3} = 10^{\frac{C_c\log\left(\frac{\alpha}{\beta}\right)-C_r\log(\sigma'_A)+\frac{1}{2\beta}\frac{\sigma'_A}{\alpha+\beta\sigma'_A}}{C_c-C_r}} \tag{22}$$

The void ratio at points C′ and C can be further obtained by substituting $\sigma' = P_c^{M3}$ (Eq 22) into the VCL (Eq 13) and the 3P-RH (Eq 1), respectively.

FIG. 3 Interpretation of the preconsolidation pressure with respect to the 3P-RH compressibility model by means of the "Silva" graphical construction or M2 (Eq 20).

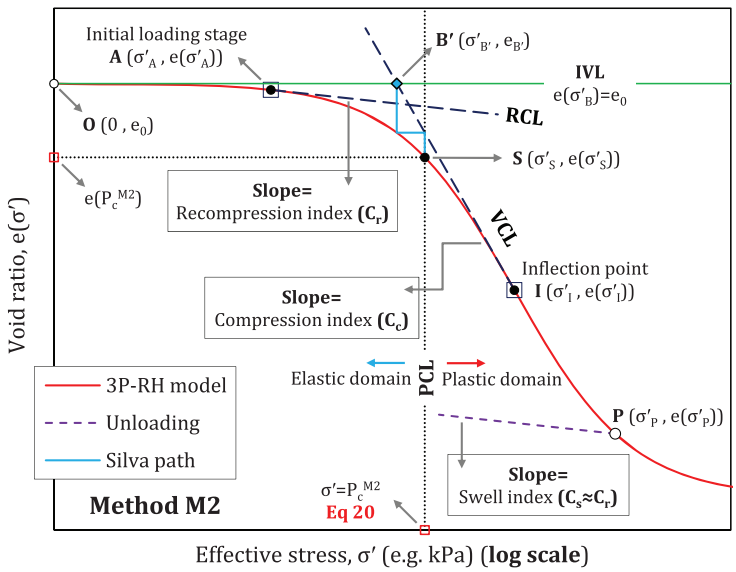

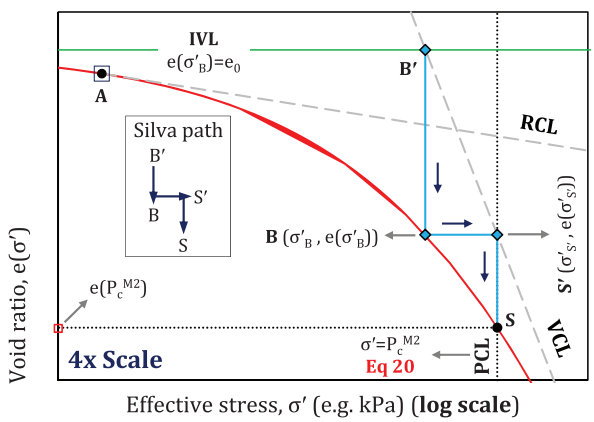

FIG. 4 Interpretation of the preconsolidation pressure with respect to the 3P-RH compressibility model by means of the "VCL-RCL Intercept" graphical construction or M3 (Eq 22).

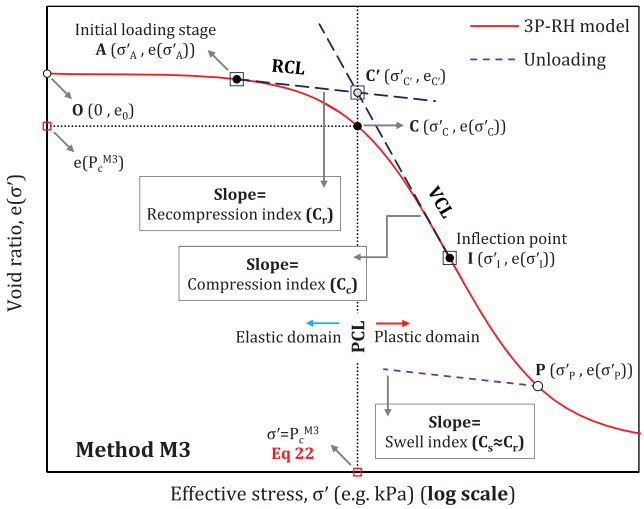

The Log-Log Method

The Log-Log construction proposed by Jose, Sridharan, and Abraham (1989) and Sridharan, Abraham, and Jose (1991) can be basically considered as a modified version of the RCL-VCL Intercept method, as it proposes an identical procedure; however, it is over the log*e*:logσ' space. On this basis, the approach may be illustrated using the same figure adopted for M3 (**Fig. 4**). The method is probably the only approach established based on prior knowledge of the preconsolidation pressure. The preconsolidation pressure in accordance with the Log-Log method (herein M4) is defined as the intersection of the newly constructed recompression and virgin compression lines over the log*e*:logσ' space (termed as $\overline{\text{RCL}}$ and $\overline{\text{VCL}}$). The approach is expected to be a less subjective one, providing that the log*e*-logσ' relationship ideally behaves as a two-segment linear function, where, in this case, P_c can be interpreted by means of a simple linear regression analysis. Sigmoidal functions including the 3P-RH, however, still remain a reversed *S*-shaped curve over the Log-Log space. As a result, the subjective difficulties may still remain current. Application of the Log-Log method is quite simple and straightforward (as M3). From a mathematical perspective, however, the Log-Log approach poses as a problem of greater complexity as both void ratio and effective stress are defined over a logarithmic scale that results in a sophisticated derivation procedure. Nonetheless, due to the simple functional form of the 3P-RH, an explicit analytical solution may still be obtained.

The inflection point (point I in **Fig. 4**) with respect to the log*e*:logσ' space can be obtained by the following three-step procedure:

$$f'_{\log} = \frac{\mathrm{d}\log e(\sigma')}{\mathrm{d}\log\sigma'} = \frac{\partial \log e(\sigma')}{\partial\sigma'} \times \sigma' \times \ln 10 = \frac{-\alpha\sigma'}{e_0(\alpha+\beta\sigma')^2 - \sigma'(\alpha+\beta\sigma')} \tag{23}$$

$$f''_{\log} = \frac{\mathrm{d}\log f'_{\log}}{\mathrm{d}\log\sigma'} = \frac{\partial \log f'_{\log}}{\partial\sigma'} \times \sigma' \times \ln 10 = \frac{e_0\alpha^2 + \beta(1-\beta e_0)\sigma'^2}{e_0(\alpha+\beta\sigma')^2 - \sigma'(\alpha+\beta\sigma')} \tag{24}$$

$$f''_{\log} = 0 : \begin{cases} \sigma'_{\mathrm{I}} = \frac{\alpha}{\beta}\sqrt{\frac{\beta e_0}{\beta e_0 - 1}}; \beta > \frac{1}{e_0} \\ e(\sigma'_{\mathrm{I}}) = e_0\sqrt{\frac{\beta e_0 - 1}{\beta e_0}} = \frac{\beta e_0}{\alpha}\sigma'_{\mathrm{I}} \end{cases} \tag{25}$$

where:

$f'_{\log}$ and $f''_{\log}$ = first and second derivatives over the log*e*: logσ' space.

Considering a similar approach adopted in the *e*:logσ' space, the new compression (C'_c) and recompression (C'_r) indices over the log*e*:logσ' space can be determined by substituting the inflection point value (Eq 25) and the user-defined point A ($\sigma' = \sigma'_{\mathrm{A}}$) into $f'_{\log}$ (Eq 23), which results in the following:

$$C'_c = \left.\frac{\mathrm{d}\log e(\sigma')}{\mathrm{d}\log\sigma'}\right|_{\sigma'=\sigma'_{\mathrm{I}}} = \frac{-1}{(\sqrt{\beta e_0} + \sqrt{\beta e_0 - 1})^2} \tag{26}$$

$$C'_r = \left.\frac{\mathrm{d}\log e(\sigma')}{\mathrm{d}\log\sigma'}\right|_{\sigma'=\sigma'_{\mathrm{A}}} = \frac{-\alpha\sigma'_{\mathrm{A}}}{e_0(\alpha+\beta\sigma'_{\mathrm{A}})^2 - \sigma'_{\mathrm{A}}(\alpha+\beta\sigma'_{\mathrm{A}})} \tag{27}$$

Considering basic geometrical relationships between C'_c and C'_r (Eqs 26 and 27, respectively) and points I (Eq 25) and A (σ'_{A},$e(\sigma'_{\mathrm{A}})$), the following can be obtained for describing the newly constructed virgin compression and recompression lines over the log*e*:logσ' space:

$$\overline{\text{VCL}}: \log e = C'_c \log\left(\frac{\beta}{\alpha}\sqrt{\frac{\beta e_0 - 1}{\beta e_0}}\sigma'\right) + \overbrace{\log\left(e_0\sqrt{\frac{\beta e_0 - 1}{\beta e_0}}\right)}^{e(\sigma'_{\mathrm{I}})} \tag{28}$$

$$\overline{\text{RCL}}: \log e = C'_r \log\left(\frac{\sigma'}{\sigma'_{\mathrm{A}}}\right) + \overbrace{\log\left(e_0 - \frac{\alpha\sigma'_{\mathrm{A}}}{\alpha+\beta\sigma'_{\mathrm{A}}}\right)}^{e(\sigma'_{\mathrm{A}})} \tag{29}$$

P_c^{M4} can now be solved by equating Eqs 28 and 29, which results in the following:

$$\sigma'_{\mathrm{C}'} = \sigma'_{\mathrm{C}} = P_c^{\mathrm{M4}} = 10^{\frac{C'_c\log\left(\frac{\alpha}{\beta}\sqrt{\frac{\beta e_0}{\beta e_0-1}}\right) - C'_r\log(\sigma'_{\mathrm{A}}) + \log\left(\frac{e_0 - \frac{\sigma'_{\mathrm{A}}}{\alpha+\beta\sigma'_{\mathrm{A}}}}{e_0\sqrt{\frac{\beta e_0-1}{\beta e_0}}}\right)}{C'_c - C'_r}} \tag{30}$$

The void ratio at point C′ and point C may also be determined by substituting $\sigma' = P_c^{\mathrm{M4}}$ (Eq 30) into the $\overline{\text{VCL}}$ (Eq 28) and the 3P-RH (Eq 1), respectively.

A practical summary of the proposed regression-aided analytical framework for determination of the compressibility curve variables by means of the 3P-RH model is presented in **Table 1**. The applicability of the proposed framework is dependent on $\sigma'_{\mathrm{I}} \leq \sigma'_{\mathrm{P}}$ (σ'_{P} is the final effective stress applied in a typical compression test as shown in **Fig. 4**), meaning that the estimated inflection point of

TABLE 1 Summary of the proposed regression-aided analytical framework for determining the compressibility curve variables.

Properties	Space	Model	Equation
3P-RH	e:σ'	$e(\sigma') = e_0 - \frac{\sigma'}{\alpha+\beta\sigma'}$	Eq 1
C_c	e:logσ'	$C_c = \frac{-\ln 10}{4\beta}$	Eq 5
	log$e$:logσ'	$C'_c = \frac{-1}{(\sqrt{\beta e_0}+\sqrt{\beta e_0 - 1})^2}; \beta > \frac{1}{e_0}$	Eq 26
C_r	e:logσ'	$C_r = \frac{-\ln 10 \alpha \sigma'_A}{(\alpha+\beta\sigma'_A)^2}$	Eq 6
	log$e$:logσ'	$C'_r = \frac{-\alpha\sigma'_A}{e_0(\alpha+\beta\sigma'_A)^2 - \sigma'_A(\alpha+\beta\sigma'_A)}$	Eq 27
Critical State Framework			
λ	e:lnσ'	$\lambda = \frac{C_c}{\ln 10} = \frac{-1}{4\beta}$	Eq 7
κ	e:lnσ'	$\kappa = \frac{C_r}{\ln 10} = \frac{-\alpha\sigma'_A}{(\alpha+\beta\sigma'_A)^2}$	Eq 8
VCL	e:logσ'	$e = e_0 + C_c \log\left(\frac{\beta}{\alpha}\sigma'\right) - \frac{1}{2\beta}$	Eq 13
RCL	e:logσ'	$e = e_0 + C_r \log\left(\frac{\sigma'}{\sigma'_A}\right) - \frac{\sigma'_A}{\alpha+\beta\sigma'_A}$	Eq 21
Preconsolidation Pressure			
M1/M1S	e:logσ'	$P_c^{M1} \approx P_c^{M1S} = \frac{\dot{e}^{-\sqrt{3}}}{\sqrt{2-\sqrt{3}}}\left(\frac{\alpha}{\beta}\right)$	Eq 17
M2	e:logσ'	$P_c^{M2} = \dot{e}^{-2\left(\frac{\dot{e}^2-1}{\dot{e}^2+1}\right)}\left(\frac{\alpha}{\beta}\right)$	Eq 20
M3	e:logσ'	$P_c^{M3} = 10^{\frac{C_c \log\left(\frac{\alpha}{\beta}\right) - C_r \log\left(\sigma'_A\right) + \frac{1}{2\beta} - \frac{\sigma'_A}{\alpha+\beta\sigma'_A}}{C_c - C_r}}$	Eq 22
M4	log$e$:logσ'	$P_c^{M4} = 10^{\frac{C'_c \log\left(\frac{\alpha}{\beta}\sqrt{\frac{\beta e_0}{\beta e_0 - 1}}\right) - C'_r \log(\sigma'_A) + \log\left(\frac{e_0 - \frac{\sigma'_A}{\alpha+\beta\sigma'_A}}{e_0\sqrt{\frac{\beta e_0 - 1}{\beta e_0}}}\right)}{C'_c - C'_r}}$	Eq 30

Notes: M1/M1S = Classical or Simplified Classical method. M2 = Silva method. M3 = RCL-VCL Intercept method. M4 = Log-Log method. $\dot{e}$ = Euler's number (≈ 2.718).

the 3P-RH function should fall in the range of measured laboratory data. Where σ'_I becomes increasingly greater than σ'_p, there is the possibility of relocating the VCL to higher stress ranges and thus overestimating the preconsolidation pressure.

Framework Validation

MODEL VALIDATION

A database of 34 compression tests was selected from the literature to validate the newly proposed 3P-RH model. Extensive care was taken to promote a database that not only covered a wide range of soils but also various testing approaches and sample preparation techniques. Index properties of the soils, including grain size analysis and consistency characteristics, accompanied by the original source of each dataset, are presented in **Table 2**. In addition, descriptive statistics of the index properties are presented in **Table 3**. According to these statistics, one can conclude that the database fairly includes a variety of soil types covering a wide range of possible index properties, hence providing a solid basis for model validation. The fitting parameters e_0, α, and β were obtained by means of the nonlinear least squares optimization technique. Since the actual value of e_0 was not reported by the majority of data sources, e_0 was set an independent fitting parameter. Statistical fit-measure indices, namely the coefficient of determination (R^2) and the normalized root mean square error ($NRMSE$) were obtained for model validation by the following:

$$(\%)\ NRMSE = \frac{100}{e(\sigma')_{a\max} - e(\sigma')_{a\min}} \overbrace{\sqrt{\frac{1}{N}\sum_{i=1}^{N}\left[e(\sigma')_{mi} - e(\sigma')_{ai}\right]^2}}^{RMSE} \quad (31)$$

where:

$e(\sigma')_{mi}$ = predicted void ratio,
$e(\sigma')_{ai}$ = actual void ratio,
$e(\sigma')_{a\ \max}$ and $e(\sigma')_{a\ \min}$ = maximum and minimum actual void ratios, and
N = number of void ratio–effective stress data points for a typical dataset (see **Table 2**).

SENSITIVITY ANALYSIS

As demonstrated in **Table 1**, the preconsolidation pressure with respect to various graphical constructions was obtained as a direct function of the fitting parameters α and β ($P_c = f(\alpha,\beta)$). To understand the influence of these parameters on the preconsolidation pressure function, a sensitivity analysis with respect to M1/M1S, M2, M3, and M4 was considered. As P_c is currently defined by means of continuous mathematical relationships, the Partial Derivative approach (quite similar to that adopted by

TABLE 2 Index properties of the soils with respect to the compiled data from the literature used for model validation.

Soil Description	No.	G_s	C	M	F_{200}	S	LL	PL	PI	USCS	Source
Drammen Lean Clay	S1	–	–	–	–	–	36	21	15	CL	Bjerrum (1967)
Drammen Plastic Clay	S2	–	–	–	–	–	59	28	31	CH	
Montmorillonite (Fat Clay)	S3	2.83	100	0	100	0	305	44	261	CH	Sridharan and Venkatappa Rao (1973)
Kaolinite (Silt)	S4	2.59	54	45	99	1	49	29	20	ML	
Black Cotton Soil (Fat Clay with Sand)	S5	2.71	29	43	72	16	101	28	73	CH	
P5D4 (Silty Sand)	S6	2.70	–	–	40	47	48	31	17	SM	Sridharan and Allam (1982)
P5D9 (Clayey Sand)	S7	2.70	–	–	18	78	40	25	15	SC	
P2D4 (Clayey Sand with Gravel)	S8	2.71	–	–	35	49	39	25	14	SC	
P2D10 (Clayey Sand)	S9	2.70	–	–	46	42	56	27	29	SC	
P7D4 (Silty Sand)	S10	2.72	–	–	49	47	45	28	17	SM	
P3D11 (Silty Sand)	S11	2.73	–	–	32	65	52	33	19	SM	
NG1 (Clayey Sand)	S12	2.60	–	–	48	49	43	26	17	SC	
NG2 (Sandy Lean Clay)	S13	2.62	–	–	61	33	45	25	20	CL	
NG3 (Clayey Sand)	S14	2.59	–	–	47	48	36	23	13	SC	
IT1 (Silty Sand)	S15	2.63	–	–	48	50	53	32	21	SM	
IT2 (Sandy Elastic Silt)	S16	2.59	–	–	52	46	51	31	20	MH	
Mg-Bentonite	S17	2.65	–	–	–	–	129	50	79	MH	Sridharan, Rao, and Murthy (1986b)
Nettoor (Fat Clay with Sand)	S18	2.64	48	31	79	21	138	48	90	CH	Jose, Sridharan, and Abraham (1988)
Meers Fault (Sandy Lean Clay)	S19	2.70	38	31	69	30	31	19	12	CL	Cetin (2000)
Meers Fault (Sandy Lean Clay)	S20	2.72	38	23	61	38	33	18	15	CL	
Degirmenlik Flysch (Fat Clay)	S21	–	33	67	100	0	68	22	46	CH	Nalbantoglu and Tuncer (2001)
Northern Karnataka (Fat Clay)	S22	–	66	32	98	2	100	42	58	CH	Subba Rao and Tripathy (2003)
Adana-Taurides (Sandy Silty Clay)	S23	2.74	26	31	57	43	24	18	6	CL-ML	Cetin (2004)
Degirmenlik (Lean Clay)	S24	2.74	35	52	87	13	37	25	12	CL	Sridharan and Gurtug (2005)
Tuzla (Fat Clay)	S25	2.78	42	48	90	10	53	28	25	CH	
Akdeniz (Fat Clay)	S26	2.75	44	45	89	11	50	28	22	CH	
Montmorillonitic Clay (Fat Clay)	S27	2.60	76	23	99	1	98	40	58	CH	
Pune	S28	2.72	–	–	–	–	71	30	41	CH	Viswanadham, Phanikumar, and Mukherjee (2009)
Chicago Clay	S29	–	–	–	–	–	30	15	15	CL	Boone (2010)
Black Cotton Soil (Fat Clay)	S30	2.70	69	27	96	3	88	36	52	CH	Nagaraj, Munnas, and Sridharan (2010)
Karaj Clay (Lean Clay)	S31	2.72	34	56	90	10	47	20	27	CL	Estabragh, Bordbar, and Javadi (2011)
Adana-Taurides (Sandy Lean Clay)	S32	2.71	36	33	69	31	36	20	16	CL	Cetin and Gökoğlu (2013)
Kaolin (Lean Clay with Sand)	S33	2.72	25	52	77	23	47	20	27	CL	Estabragh et al. (2014)
Kaolin and Bentonite (Fat Clay with Sand)	S34	2.75	45	35	80	20	81	28	53	CH	

Notes: G_s = Specific gravity. C = Clay (<2 μm) (%). M = Silt (2–75 μm) (%). S = Sand (0.075–4.75 mm) (%). F_{200} = Passing sieve No. 200 (<75 μm) (%). LL = Liquid limit (%). PL = Plastic limit (%). PI = Plasticity index (= LL–PL) (%). USCS = Unified soil classification (ASTM D2487-11, *Standard Practice for Classification of Soils for Engineering Purposes [Unified Soil Classification System]*).

Estabragh, Soltani, and Javadi [2016]) may be the most suitable sensitivity analysis technique. Assuming α and β as x_i, the relative impact of the independent variable x_i on the dependent variable P_c (Eqs 17, 20, 22, and 30 for M1/M1S to M4, respectively), referred to as sensitivity or S_{x_i}, can be defined as the following:

$$S_{x_i} = \frac{\sigma_{x_i}}{n\sigma_{P_c}} \sum_{j=1}^{n} \left| \frac{\partial P_c}{\partial x_i} \right|_j \tag{32}$$

where:

$\frac{\partial P_c}{\partial x_i}$ = partial derivative of the preconsolidation pressure function with respect to x_i and

σ_{P_c} and σ_{x_i} = standard deviation of the predicted preconsolidation pressure and x_i data.

The term $\partial P_c/\partial x_i$ in Eq 32 represents the likelihood of P_c increasing or decreasing as a result of increase in x_i. Hence, the likelihood of increase ($p^+_{x_i}$) or decrease ($p^-_{x_i}$) in P_c in the case of increase in x_i can be given as the following:

$$(\%)p^+_{x_i} = \frac{m^+_{x_i}}{n} \times 100 \tag{33}$$

$$(\%)p^-_{x_i} = \frac{m^-_{x_i}}{n} \times 100 \tag{34}$$

TABLE 3 Descriptive statistics of the soil index properties with respect to the compiled data from the literature.

Properties	Descriptive Statistics				
	N_a	Min	Mean	Max	σ
Specific Gravity, G_s	29	2.59	2.69	2.83	0.06
Clay (<2 μm), C (%)	18	25	46.44	100	19.73
Silt (2–75 μm), M (%)	18	0	37.56	67	15.32
Passing Sieve No. 200 (<75 μm), F_{200} (%)	29	18	68.55	100	23.91
Sand (0.075–4.75 mm), S (%)	29	0	28.59	78	21.59
Liquid Limit, LL (%)	34	24	65.22	305	50.66
Plastic Limit, PL (%)	34	13	28.07	50	8.82
Plasticity Index, PI (%)	34	6	37.15	261	44.84

Notes: N_a = Number of available data. σ = Standard deviation.

where:

$m_{x_i}^+$ and $m_{x_i}^-$ = number of observations where $\partial P_c/\partial x_i > 0$ and $\partial P_c/\partial x_i < 0$, and

n = number of void ratio–effective stress datasets, $n = 34$.

The positive and negative magnitudes ($\mu_{x_i}^+$ and $\mu_{x_i}^-$, respectively) on P_c caused by increase in x_i can be defined as the following:

$$\mu_{x_i}^+ = \frac{\sigma_{x_i}}{n\sigma_{P_c}} \sum_{j=1}^{n} \left| \frac{\partial P_c}{\partial x_i} \right|_j ; \forall x_i \ni \frac{\partial P_c}{\partial x_i} > 0 \quad (35)$$

$$\mu_{x_i}^- = \frac{\sigma_{x_i}}{n\sigma_{P_c}} \sum_{j=1}^{n} \left| \frac{\partial P_c}{\partial x_i} \right|_j ; \forall x_i \ni \frac{\partial P_c}{\partial x_i} < 0 \quad (36)$$

PROBABILISTIC COMPARISON

Because the proposed regression-aided analytical equations are able to overcome the subjective uncertainty associated with determining P_c, an accurate comparison among various graphical constructions may now be obtained. The likelihood of a particular graphical construction, say Mi, promoting a greater P_c value to that of Mj, termed as p_{ij}, can be obtained by the following:

$$(\%)p_{ij} = \frac{m_{ij}}{n} \times 100 \quad (37)$$

where:

m_{ij} = number of observations where $P_c^{Mi} > P_c^{Mj}$.

Results and Discussion

The fitting parameters (e_0, α, and β) and statistical fit-measure indices (R^2, *RMSE*, and *NRMSE*) with respect to the 3P-RH model are presented in **Table 4**. As demonstrated in the table, the 3P-RH well represents the experimental void ratio–effective stress relationship. The high R^2 and low *RMSE* or *NRMSE* values imply a high agreement between actual and predicted data, both in terms of correlation and error. The R^2 values were mainly above the 0.99 margin, meaning that nearly 99 % of variations in experimental observations are being explained by the 3P-RH. The *NRMSE* was observed to be lower than 5.00 % for the majority of cases. Results justify the high capability of the 3P-RH in describing the void ratio–effective stress relationship over a variety of scenarios.

Table 5 presents the preconsolidation pressure determined in accordance with the proposed analytical equations for M1/M1S, M2, M3, and M4 (equations presented in **Table 1**). P_c^{M1} (Eq 15) and P_c^{M1S} (Eq 17) resulted in nearly identical P_c values. Therefore, the less complex P_c^{M1S} function can replace the more sophisticated P_c^{M1} for defining the preconsolidation pressure in accordance with the Classical method. **Table 6** presents a probabilistic comparison of the preconsolidation pressure value with respect to various graphical constructions. For instance, the likelihood of M1/M1S promoting a greater preconsolidation pressure compared to that of M2, M3, and M4 was determined (by Eq 37) as 100 %, 100 %, and 97.06 %, respectively. Based on the probabilistic data, the graphical constructions may be ranked in order as $P_c^{M1/M1S} > P_c^{M4} \geq P_c^{M2} > P_c^{M3}$, with methods M4 and M2 showing marginal differences for the majority of cases.

A summary of the sensitivity analysis results for α and β with respect to the preconsolidation pressure functions $P_c^{M1/M1S}$, P_c^{M2}, P_c^{M3}, and P_c^{M4} (equations presented in **Table 1**) is presented in **Table 7**. A review of the sensitivity parameter S_{x_i} indicates that the variations of P_c are mainly controlled and dominated by the fitting parameter α. All S_{x_i} values for α were observed to be significantly greater than those determined for β ($S_\alpha > S_\beta$). Regarding methods M1/M1S, M2, and M3, the sensitivity parameter S_α was observed to be approximately four times greater than S_β ($S_\alpha/S_\beta \approx 4$). In the case of M4, however, S_α/S_β was nearly 2, meaning that the P_c^{M4} function is relatively more sensitive to the variations of β compared to others. The likelihood of increase

TABLE 4 Summary of the regression analysis outputs with respect to the 3P-RH compressibility model (Eq 1) for the compiled data from the literature.

No.	N	e_0	α (kPa)	β	R^2	*RMSE*	*NRMSE* (%)
S1	10	0.974	690.77	2.394	0.9838	1.17×10^{-2}	4.66
S2	10	1.488	405.32	1.093	0.9817	2.68×10^{-2}	5.04
S3	9	4.959	60.09	0.258	0.9978	4.62×10^{-2}	1.64
S4	8	0.961	732.40	3.457	0.9962	4.73×10^{-3}	2.21
S5	8	1.183	517.02	1.301	0.9908	1.71×10^{-2}	3.54
S6	7	0.767	957.02	3.477	0.9983	2.36×10^{-3}	1.48
S7	7	0.876	570.08	2.788	0.9990	2.30×10^{-3}	1.01
S8	7	0.803	674.75	3.167	0.9932	5.73×10^{-3}	2.93
S9	7	0.858	1,398.14	4.765	0.9989	1.32×10^{-3}	1.15
S10	7	0.669	997.76	3.780	0.9977	2.54×10^{-3}	1.69
S11	7	0.811	894.55	3.202	0.9978	2.86×10^{-3}	1.59
S12	8	0.602	1,185.74	3.632	0.9968	3.75×10^{-3}	1.89
S13	8	0.718	707.68	3.077	0.9966	4.98×10^{-3}	1.97
S14	8	0.599	981.47	3.958	0.9966	3.85×10^{-3}	1.96
S15	7	0.702	708.11	4.224	0.9985	2.12×10^{-3}	1.35
S16	7	0.763	604.12	3.147	0.9948	5.15×10^{-3}	2.43
S17	7	2.439	113.08	0.569	0.9981	1.85×10^{-2}	1.53
S18	7	4.014	37.51	0.293	0.9938	7.08×10^{-2}	2.92
S19	10	0.776	8,728.39	6.119	0.9912	2.63×10^{-3}	2.99
S20	12	0.773	6,931.63	5.536	0.9904	2.97×10^{-3}	2.90
S21	8	0.882	713.56	2.236	0.9982	5.44×10^{-3}	1.48
S22	8	1.205	2,943.35	6.487	0.9947	2.38×10^{-3}	2.40
S23	15	0.798	753.96	2.166	0.9994	2.47×10^{-3}	0.76
S24	7	0.583	2,945.14	4.006	0.9978	2.68×10^{-3}	1.58
S25	7	0.821	1,618.23	2.349	0.9985	3.91×10^{-3}	1.31
S26	7	0.745	2,075.23	2.829	0.9983	3.35×10^{-3}	1.41
S27	7	1.148	896.32	1.812	0.9985	5.41×10^{-3}	1.32
S28	8	0.937	735.95	2.127	0.9962	6.59×10^{-3}	2.21
S29	16	0.629	2,182.14	2.863	0.9990	2.48×10^{-3}	0.89
S30	9	1.582	433.55	1.071	0.9989	8.54×10^{-3}	1.20
S31	6	1.897	156.26	2.183	0.9987	3.17×10^{-3}	1.33
S32	16	0.864	46.31	1.535	0.9986	6.92×10^{-3}	1.24
S33	8	2.095	380.86	1.577	0.9968	1.05×10^{-2}	1.98
S34	8	3.219	217.16	0.738	0.9941	2.99×10^{-2}	2.90
	ΣN = 291						

Note: N = Number of void ratio–effective stress data points.

in P_c as a result of increase in α was observed to be 100 % with respect to all methods ($p_\alpha^+ = 100\%$), which suggests a direct relationship between α and P_c ($P_c \sim \alpha$). On the contrary, β inversely influences P_c ($P_c \sim \beta^{-1}$), as the likelihood of decrease in P_c owing to increase in β was observed to be 100 % ($p_\beta^- = 100\,\%$). The magnitude of increase ($\mu_{x_i}^+$) and decrease ($\mu_{x_i}^-$) in P_c as a result of increase in α and β suggests equal values to that of S_{x_i}. A comparison of the sensitivity and magnitude values presented in **Table 7** indicates that while methods M1/M1S, M2, and M3 more or less show similar sensitivities to α and β, M4 is quite more sensitive to the variations of α and β. Therefore, the accuracy of the determined preconsolidation pressure by means of M4 (Eq 30) may be more dependent on how well the 3P-RH simulates experimental data.

Applications

The conventional oedometer test (ASTM D2435-11, *Standard Test Methods for One-Dimensional Consolidation Properties of Soils Using Incremental Loading*, and ASTM D4546-14, *Standard Test Methods for One-Dimensional Swell or Collapse of Soils*) has been widely criticized as a relatively time-consuming process. With the

TABLE 5 Preconsolidation pressure with respect to the proposed regression-aided analytical equations for various graphical constructions.

No.	P_c^{M1} (kPa) (Eq 15)	P_c^{M1S} (kPa) (Eq 17)	P_c^{M2} (kPa) (Eq 20)	P_c^{M3} (kPa) (Eq 22)	P_c^{M4} (kPa) (Eq 30)
S1	98.56	98.64	62.92	68.93	82.76
S2	126.28	126.72	80.83	81.02	112.25
S3	77.12	79.49	50.70	43.21	75.18
S4	72.39	72.42	46.20	39.07	44.92
S5	135.49	135.83	86.64	66.39	101.04
S6	94.05	94.08	60.01	48.63	58.66
S7	69.86	69.89	44.58	38.65	47.23
S8	72.78	72.82	46.45	39.44	47.84
S9	100.27	100.29	63.97	50.98	57.15
S10	90.18	90.21	57.54	46.98	57.34
S11	95.46	95.50	60.92	49.17	59.71
S12	111.55	111.59	71.18	55.68	71.36
S13	78.57	78.61	50.14	42.09	53.15
S14	84.72	84.74	54.06	44.66	55.36
S15	57.29	57.30	36.55	33.00	38.45
S16	65.59	65.62	41.86	36.70	44.97
S17	67.16	67.89	43.31	37.60	59.99
S18	42.61	43.76	27.91	25.41	48.88
S19	487.46	487.52	310.98	250.75	275.94
S20	427.87	427.93	272.97	226.51	251.70
S21	108.96	109.06	69.56	55.96	74.07
S22	155.06	155.08	98.92	74.28	78.76
S23	118.89	119.00	75.91	48.65	72.01
S24	251.22	251.29	160.29	114.77	146.10
S25	235.26	235.45	150.18	108.67	148.08
S26	250.60	250.74	159.94	114.95	151.40
S27	168.83	169.06	107.84	81.22	106.59
S28	118.13	118.24	75.42	53.40	72.08
S29	260.36	260.50	166.17	126.76	176.33
S30	137.86	138.36	88.25	67.21	96.53
S31	24.44	24.46	15.60	14.51	16.05
S32	10.29	10.31	6.58	4.56	8.15
S33	82.41	82.56	52.66	40.45	47.00
S34	99.88	100.59	64.16	47.94	60.30

TABLE 6 Probabilistic comparison of the preconsolidation pressure with respect to various graphical constructions.

		Mj			
	Method	M1/M1S	M2	M3	M4
Mi	M1/M1S	—	100	100	97.06
	M2	0	—	94.12	47.06
	M3	0	5.88	—	0
	M4	2.94	52.94	100	—

Note: Values represent the likelihood of M*i* promoting a greater preconsolidation pressure compared to that of M*j* (%).

TABLE 7 Summary of the sensitivity analysis results for the fitting parameters α and β with respect to various preconsolidation pressure functions.

x_i	Method	$\frac{\partial P_c}{\partial x_i}$	$\frac{1}{n}\sum_{j=1}^{n}\left\|\frac{\partial P_c}{\partial x_i}\right\|_j$	σ_{x_i}	σ_{P_c}(kPa)	$\frac{\sigma_{x_i}}{\sigma_{P_c}}$	S_{x_i}	$m^+_{x_i}$	$p^+_{x_i}$(%)	$m^-_{x_i}$	$p^-_{x_i}$(%)	$\mu^+_{x_i}$	$\mu^-_{x_i}$
Fitting Parameter α	M1/M1S (Eq 17)	$\frac{\dot{e}^{-\sqrt{3}}}{\sqrt{2-\sqrt{3}}}\left(\frac{1}{\beta}\right)$	0.23	1,824.14	102.97	17.72	3.99	34	100	0	0	3.99	0
	M2 (Eq 20)	$\dot{e}^{-2\left(\frac{\dot{e}^2-1}{\dot{e}^2+1}\right)}\left(\frac{1}{\beta}\right)$	0.14	1,824.14	65.68	27.77	3.99	34	100	0	0	3.99	0
	M3 (Eq 22)	Eq A1	0.10	1,824.14	51.66	35.31	3.37	34	100	0	0	3.37	0
	M4 (Eq 30)	Eq A2	0.15	1,824.14	58.95	30.94	4.73	34	100	0	0	4.73	0
Fitting Parameter β	M1/M1S (Eq 17)	$-\frac{\dot{e}^{-\sqrt{3}}}{\sqrt{2-\sqrt{3}}}\left(\frac{\alpha}{\beta^2}\right)$	65.66	1.56	102.97	0.015	0.99	0	0	34	100	0	0.99
	M2 (Eq 20)	$-\dot{e}^{-2\left(\frac{\dot{e}^2-1}{\dot{e}^2+1}\right)}\left(\frac{\alpha}{\beta^2}\right)$	41.88	1.56	65.68	0.024	0.99	0	0	34	100	0	0.99
	M3 (Eq 22)	Eq A3	27.63	1.56	51.66	0.030	0.83	0	0	34	100	0	0.83
	M4 (Eq 30)	Eq A4	74.79	1.56	58.95	0.026	1.97	0	0	34	100	0	1.97

Note: $\dot{e}$ = Euler's number ($\approx$ 2.718).

goal of avoiding the labor of such tests, numerous attempts have been made to estimate the compressibility curve variables C_c and C_r as a function of the soil's index properties (e.g., consistency characteristics) by means of various data-driven techniques. The existing empirical models can be generally divided into two categories based on the adopted technique used for model development, namely, traditional (classical statistical analyses) and nontraditional (computational intelligence methods). A more detailed discussion may be found in Onyejekwe, Kang, and Ge (2014), Kordnaeij et al. (2015), and Moayed, Kordnaeij, and Mola-Abasi (2016). C_c was defined as a function of β (Eq 5); hence, by predicting C_c in accordance with any well-established empirical model, β can be obtained. Since C_r was expressed as a function of α and β (Eq 6), predicting C_r by any chosen empirical relationship, α can be estimated with a known β. This implies that by integrating the existing empirical models for C_c and C_r with Eqs 5 and 6, it is possible to construct the compressibility curve (and determine P_c) without the need of conducting oedometer tests, which would be quite useful, particularly for initial estimations. The validity of the constructed compressibility curve, however, strongly relies on how well the selected empirical models are able to predict C_c and C_r. Hence, the first essential step is to review the applicability conditions of each empirical relationship and select a model that best suits the study objectives.

Conclusions

The following conclusions could be drawn from this study:

1. The proposed 3P-RH compressibility model accompanied by the suggested analytical solutions for solving the compressibility curve variables construct a unique framework for modeling the compressibility behavior of soils with an acceptable degree of accuracy and, more importantly, by a simple objective approach. Utilization of the framework relies on estimation of the fitting parameters α and β, which are normally determined by means of void ratio–effective stress oedometer data or alternatively predicted by the well-established empirical relationships proposed for C_c and C_r.
2. The subjective judgement and uncertainty associated with defining the preconsolidation pressure over the e:logσ' or log$e$:logσ' space can be avoided or at least minimized by introducing a continuous mathematical function that involves physically meaningful parameters. Based on the probabilistic comparison, the investigated graphical constructions may be ranked in order as $P_c^{\mathrm{M1/M1S}} > P_c^{\mathrm{M4}} \geq P_c^{\mathrm{M2}} > P_c^{\mathrm{M3}}$. The sensitivity analysis indicated that the preconsolidation function obtained in accordance with the Log-Log method (P_c^{M4}) is much more sensitive to the variations of α and β.

ACKNOWLEDGMENTS

The authors wish to thank the reviewers for their contributions and suggestions, which have significantly added to the clarity and value of the paper. This research was funded by the Australian Research Council (ARC) via project No. DP140103004, and their support is gratefully acknowledged.

Appendix

The Wolfram Mathematica 10.2 software package was used to determine the first derivative of the M3 and M4 preconsolidation pressure functions (Eqs 22 and 30, respectively) with respect to α and β ($\partial P_c/\partial\alpha$ and $\partial P_c/\partial\beta$), which resulted in the following:

$$\mathbf{M3}: \frac{\partial P_c}{\partial \alpha} = \frac{10^{\frac{(\alpha+A\beta)\left(-2\alpha+2A\beta+(\alpha+A\beta)Ln\left[\frac{\alpha}{\beta}\right]\right)}{(\alpha-A\beta)^2\mathrm{Ln}[10]}} A^{-\frac{4A\alpha\beta}{(\alpha-A\beta)^2}}((\alpha-A\beta)(\alpha^2+6A\alpha\beta+A^2\beta^2)+4A\alpha\beta(\alpha+A\beta)\left(\mathrm{Ln}[A]-\mathrm{Ln}\left[\frac{\alpha}{\beta}\right]\right))}{\alpha(\alpha-A\beta)^3} \tag{A1}$$

$$\mathbf{M3}: \frac{\partial P_c}{\partial \beta} = \frac{10^{\frac{(\alpha+A\beta)(-2\alpha+2A\beta+(\alpha+A\beta)Ln[\frac{\alpha}{\beta}])}{(\alpha-A\beta)^2\mathrm{Ln}[10]}} A^{-\frac{4A\alpha\beta}{(\alpha-A\beta)^2}}((\alpha-A\beta)(\alpha^2+6A\alpha\beta+A^2\beta^2)+4A\alpha\beta(\alpha+A\beta)\left(\mathrm{Ln}[A]-\mathrm{Ln}\left[\frac{\alpha}{\beta}\right]\right))}{\beta(-\alpha+A\beta)^3} \tag{A2}$$

$$\mathbf{M4}: \frac{\partial P_c}{\partial \alpha} = \frac{1}{\left(\frac{1}{\left(\sqrt{\beta e}+\sqrt{\beta e-1}\right)^2}-\frac{\alpha A}{e(\alpha+A\beta)^2-A(\alpha+A\beta)}\right)^2} 10^{\frac{\frac{\alpha A\mathrm{LN}[A]}{e(\alpha+A\beta)^2-A(\alpha+A\beta)}+\mathrm{LN}\left[\frac{e-\frac{A}{\alpha+A\beta}}{e\sqrt{1-\frac{1}{\beta e}}}\right]-\frac{\mathrm{LN}\left[\frac{\alpha\sqrt{\frac{1}{\beta e-1}+1}}{\beta}\right]}{\left(\sqrt{\beta e}+\sqrt{\beta e-1}\right)^2}}{\mathrm{LN}[10]\left(\frac{\alpha A}{e(\alpha+A\beta)^2-A(\alpha+A\beta)}-\frac{1}{\left(\sqrt{\beta e}+\sqrt{\beta e-1}\right)^2}\right)}}$$

$$\left(\left(\frac{\alpha A}{e(\alpha+A\beta)^2-A(\alpha+A\beta)}-\frac{1}{(\sqrt{\beta e}+\sqrt{\beta e-1})^2}\right)\left(\frac{\mathrm{LN}[A](A^3\beta(\beta e-1)-\alpha^2 Ae)}{(\alpha+A\beta)^2(A(\beta e-1)+\alpha e)^2}+\frac{A}{(\alpha+A\beta)(A\beta e-A+\alpha e)}-\frac{1}{\alpha(\sqrt{\beta e}+\sqrt{\beta e-1})^2}\right)\right.$$

$$\left.-\frac{(A^3\beta(\beta e-1)-\alpha^2 Ae)\left(\frac{\alpha A\mathrm{LN}[A]}{e(\alpha+A\beta)^2-A(\alpha+A\beta)}+\mathrm{LN}\left[\frac{e-\frac{A}{\alpha+A\beta}}{e\sqrt{1-\frac{1}{\beta e}}}\right]-\frac{\mathrm{LN}\left[\frac{\alpha\sqrt{\frac{1}{\beta e-1}+1}}{\beta}\right]}{\left(\sqrt{\beta e}+\sqrt{\beta e-1}\right)^2}\right)}{(\alpha+A\beta)^2(A(\beta e-1)+\alpha e)^2}\right). \tag{A3}$$

$$\mathbf{M4}: \frac{\partial P_c}{\partial \beta} = \frac{1}{\left(-\frac{A\alpha}{-A(\alpha+A\beta)+e(\alpha+A\beta)^2}+\frac{1}{\left(\sqrt{e\beta}+\sqrt{-1+e\beta}\right)^2}\right)^2} 10^{\frac{\frac{A\alpha\mathrm{LN}[A]}{-A(\alpha+A\beta)+e(\alpha+A\beta)^2}+\mathrm{LN}\left[\frac{e-\frac{A}{\alpha+A\beta}}{e\sqrt{1-\frac{1}{e\beta}}}\right]-\frac{\mathrm{LN}\left[\frac{\alpha\sqrt{1+\frac{1}{-1+e\beta}}}{\beta}\right]}{\left(\sqrt{e\beta}+\sqrt{-1+e\beta}\right)^2}}{\left(\frac{A\alpha}{-A(\alpha+A\beta)+e(\alpha+A\beta)^2}-\frac{1}{\left(\sqrt{e\beta}+\sqrt{-1+e\beta}\right)^2}\right)\mathrm{LN}[10]}}$$

$$\left(-\left(\frac{A\alpha}{(\alpha+A\beta)^2}+e\left(-2+\frac{1}{\sqrt{1-\frac{1}{e\beta}}}+\sqrt{1-\frac{1}{e\beta}}-\frac{Ae\alpha}{(e\alpha+A(-1+e\beta))^2}\right)\right)\left(\frac{A\alpha\mathrm{LN}[A]}{-A(\alpha+A\beta)+e(\alpha+A\beta)^2}+\mathrm{LN}\left[\frac{e-\frac{A}{\alpha+A\beta}}{e\sqrt{1-\frac{1}{e\beta}}}\right]-\frac{\mathrm{LN}\left[\frac{\alpha\sqrt{1+\frac{1}{-1+e\beta}}}{\beta}\right]}{(\sqrt{e\beta}+\sqrt{-1+e\beta})^2}\right)\right.$$

$$+\frac{1}{2}\left(\frac{A\alpha}{-A(\alpha+A\beta)+e(\alpha+A\beta)^2}-\frac{1}{(\sqrt{e\beta}+\sqrt{-1+e\beta})^2}\right)\left(4e-\frac{2e}{\sqrt{1-\frac{1}{e\beta}}}-2e\sqrt{1-\frac{1}{e\beta}}-\frac{2A}{\alpha+A\beta}+\frac{2Ae}{e\alpha+A(-1+e\beta)}\right.$$

$$\left.\left.+\frac{2A^2\alpha(A-2e\alpha-2Ae\beta)\mathrm{LN}[A]}{(\alpha+A\beta)^2(e\alpha+A(-1+e\beta))^2}+\frac{2\mathrm{LN}[\frac{\alpha\sqrt{1+\frac{1}{-1+e\beta}}}{\beta}]}{\sqrt{1-\frac{1}{e\beta}}\,\beta(\sqrt{e\beta}+\sqrt{-1+e}}\right)\right) \tag{A4}$$

where:

e = initial void ratio, $e = e_0$, and

A = initial effective stress at the initial loading stage or point A, $A = \sigma'_A$.

References

Alonso, E. E., Romero, E., Hoffmann, C., and García-Escudero, E., 2005, "Expansive Bentonite–Sand Mixtures in Cyclic Controlled-Suction Drying and Wetting," *Eng. Geol.*, Vol. 81, No. 3, pp. 213–226, https://doi.org/10.1016/j.enggeo.2005.06.009

Al-Shamrani, M. A., 2005, "Applying the Hyperbolic Method and Cα/Cc Concept for Settlement Prediction of Complex Organic-Rich Soil Formations," *Eng. Geol.*, Vol. 77, Nos. 1–2, pp. 17–34, https://doi.org/10.1016/j.enggeo.2004.07.004

Arvidsson, J. and Keller, T., 2004, "Soil Precompression Stress: I. A Survey of Swedish Arable Soils," *Soil Tillage Res.*, Vol. 77, No. 1, pp. 85–95, https://doi.org/10.1016/j.still.2004.01.003

ASTM D2435/D2435M-11, 2010, *Standard Test Methods for One-Dimensional Consolidation Properties of Soils Using Incremental Loading*, ASTM International, West Conshohocken, PA, www.astm.org

ASTM D2487-11, 2011, *Standard Practice for Classification of Soils for Engineering Purposes (Unified Soil Classification System)*, ASTM International, West Conshohocken, PA, www.astm.org

ASTM D4546-14, 2014, *Standard Test Methods for One-Dimensional Swell or Collapse of Soils*, ASTM International, West Conshohocken, PA, www.astm.org

Baumgartl, T. and Köck, B., 2004, "Modeling Volume Change and Mechanical Properties with Hydraulic Models," *Soil Sci. Soc. Am. J.*, Vol. 68, No. 1, pp. 57–65, https://doi.org/10.2136/sssaj2004.5700

Becker, D. E., Crooks, J. H. A., Been, K., and Jefferies, M. G., 1987, "Work as a Criterion for Determining In Situ and Yield Stresses in Clays," *Can. Geotech. J.*, Vol. 24, No. 4, pp. 549–564, https://doi.org/10.1139/t87-070

Bjerrum, L., 1967, "Engineering Geology of Norwegian Normally-Consolidated Marine Clays as Related to Settlements of Buildings," *Géotechnique*, Vol. 17, No. 2, pp. 83–118, https://doi.org/10.1680/geot.1967.17.2.83

Boone, S. J., 2010, "A Critical Reappraisal of "Preconsolidation Pressure" Interpretations Using the Oedometer Test," *Can. Geotech. J.*, Vol. 47, No. 3, pp. 281–296, https://doi.org/10.1139/T09-093

Boscardin, B. M. D., Selig, E. T., Lin, R., and Yang, G., 1990, "Hyperbolic Parameters for Compacted Soils," *J. Geotech. Eng.*, Vol. 116, No. 1, pp. 88–104, https://doi.org/10.1061/(ASCE)0733-9410(1990)116:1(88)

Burland, J. B., 1990, "On the Compressibility and Shear Strength of Natural Clays," *Géotechnique*, Vol. 40, No. 3, pp. 329–378, https://doi.org/10.1680/geot.1990.40.3.329

Butterfield, R., 1979, "A Natural Compression Law for Soils (an Advance on e-log p′)," *Géotechnique*, Vol. 29, No. 4, pp. 469–480, https://doi.org/10.1680/geot.1979.29.4.469

Cargill, K. W., 1984, "Prediction of Consolidation of Very Soft Soil," *J. Geotech. Eng.*, Vol. 110, No. 6, pp. 775–795, https://doi.org/10.1061/(ASCE)0733-9410(1984)110:6(775)

Casagrande, A., 1936, "The Determination of Preconsolidation Load and its Practical Significance," presented at the *First International Conference on Soil Mechanics and Foundation Engineering*, Cambridge, MA, *American Society of Civil Engineers*, Reston, VA.

Cetin, H., 2000, "An Experimental Study of Soil Memory and Preconsolidation Adjacent to an Active Tectonic Structure: The Meers Fault, Oklahoma, USA," *Eng. Geol.*, Vol. 57, Nos. 3–4, pp. 169–178, https://doi.org/10.1016/S0013-7952(00)00026-0

Cetin, H., 2004, "Soil-Particle and Pore Orientations during Consolidation of Cohesive Soils," *Eng. Geol.*, Vol. 73, Nos. 1–2, pp. 1–11, https://doi.org/10.1016/j.enggeo.2003.11.006

Cetin, H. and Gökoğlu, A., 2013, "Soil Structure Changes during Drained and Undrained Triaxial Shear of a Clayey Soil," *Soils Found.*, Vol. 53, No. 5, pp. 628–638, https://doi.org/10.1016/j.sandf.2013.08.002

Chong, S. and Santamarina, J. C., 2016, "Soil Compressibility Models for a Wide Stress Range," *J. Geotech. Geoenviron. Eng.*, Vol. 142, No. 6, 6016003–7, https://doi.org/10.1061/(ASCE)GT.1943-5606.0001482

Clementino, R., 2005, "Discussion of 'An Oedometer Test Study on the Preconsolidation Stress of Glaciomarine Clays,'" *Can. Geotech. J.*, Vol. 42, No. 3, pp. 972–974, https://doi.org/10.1139/T09-093

Cui, Y. J. and Delage, P., 1996, "Yielding and Plastic Behaviour of an Unsaturated Compacted Silt," *Géotechnique*, Vol. 46, No. 2, pp. 291–311, https://doi.org/10.1680/geot.1996.46.2.291

Dias Junior, M. S. and Pierce, F. J., 1995, "A Simple Procedure for Estimating Preconsolidation Pressure from Soil Compression Curves," *Soil Technol.*, Vol. 8, No. 2, pp. 139–151, https://doi.org/10.1016/0933-3630(95)00015-8

Duncan, J. M. and Chang, C. Y., 1970, "Nonlinear Analysis of Stress and Strain in Soils," *J. Soil Mech. Found. Div.*, Vol. 96, No. 5, pp. 1629–1653.

Estabragh, A. R., Beytolahpour, I., Moradi, M., and Javadi, A. A., 2014, "Consolidation Behavior of Two Fine-Grained Soils Contaminated by Glycerol and Ethanol," *Eng. Geol.*, Vol. 178, pp. 102–108, https://doi.org/10.1016/j.enggeo.2014.05.017

Estabragh, A. R., Bordbar, A. T., and Javadi, A. A., 2011, "Mechanical Behavior of a Clay Soil Reinforced with Nylon Fibers," *Geotech. Geol. Eng.*, Vol. 29, No. 5, pp. 899–908, https://doi.org/10.1007/s10706-011-9427-8

Estabragh, A. R. and Javadi, A. A., 2013, "Roscoe and Hvorslev Surfaces for Unsaturated Silty Soil," *Int. J. Geomech.*, Vol. 14, No. 2, pp. 230–238, https://doi.org/10.1061/(ASCE)GM.1943-5622.0000306

Estabragh, A. R., Soltani, A., and Javadi, A. A., 2016, "Models for Predicting the Seepage Velocity and Seepage Force in a Fiber Reinforced Silty Soil," *Comput. Geotech.*, Vol. 75, pp. 174–181, https://doi.org/10.1016/j.compgeo.2016.02.002

Gregory, A. S., Whalley, W. R., Watts, C. W., Bird, N. R. A., Hallett, P. D., and Whitmore, A. P., 2006, "Calculation of the Compression Index and Precompression Stress from Soil Compression Test Data," *Soil Tillage Res.*, Vol. 89, No. 1, pp. 45–57, https://doi.org/10.1016/j.still.2005.06.012

Grozic, J. L. H., Lunne, T., and Pande, S., 2003, "An Oedometer Test Study on the Preconsolidation Stress of Glaciomarine Clays," *Can. Geotech. J.*, Vol. 40, No. 5, pp. 857–872, https://doi.org/10.1139/t03-043

Houlsby, G. T. and Wroth, C. P., 1991, "The Variation of Shear Modulus of a Clay with Pressure and Overconsolidation Ratio," *Soils Found.*, Vol. 31, No. 3, pp. 138–143, https://doi.org/10.3208/sandf1972.31.3_138

Imhoff, S., Da Silva, A. P., and Fallow, D., 2004, "Susceptibility to Compaction, Load Support Capacity, and Soil Compressibility of Hapludox," *Soil Sci. Soc. Am. J.*, Vol. 68, No. 1, pp. 17–24, https://doi.org/10.2136/sssaj2004.1700

Janbu, N., 1969, "The Resistance Concept Applied to Deformation of Soils," presented at the *Seventh International Conference on Soil Mechanics and Foundation Engineering*, Mexico City, Mexico, International Society for Soil Mechanics and Geotechnical Engineering, London, England.

Jose, B., Sridharan, A., and Abraham, B., 1989, "Log-Log Method for Determination of Preconsolidation Pressure," *Geotech. Test. J.*, Vol. 12, No. 3, pp. 230–237, https://doi.org/10.1520/GTJ10974J

Jose, B. T., Sridharan, A., and Abraham, B. M., 1988, "A Study of Geotechnical Properties of Cochin Marine Clays," *Mar. Geotechnol.*, Vol. 7, No. 3, pp. 189–209, https://doi.org/10.1080/10641198809388216

Kordnaeij, A., Kalantary, F., Kordtabar, B., and Mola-Abasi, H., 2015, "Prediction of Recompression Index Using GMDH-Type Neural Network Based on Geotechnical Soil Properties," *Soils Found.*, Vol. 55, No. 6, pp. 1335–1345, https://doi.org/10.1016/j.sandf.2015.10.001

Ku, T. and Mayne, P. W., 2013, "Yield Stress History Evaluated from Paired In-Situ Shear Moduli of Different Modes," *Eng. Geol.*, Vol. 152, No. 1, pp. 122–132, https://doi.org/10.1016/j.enggeo.2012.11.001

Ladd, C. C. and Foott, R., 1974, "New Design Procedure for Stability of Soft Clays," *J. Geotech. Eng. Div.*, Vol. 100, No. 7, pp. 763–786, https://doi.org/10.1016/0148-9062(74)90494-x

Liu, M. D., Xu, K. J., and Horpibulsuk, S., 2013, "A Mathematical Function to Represent S-Shaped Relationships for Geotechnical Applications," *Geotech. Eng.*, Vol. 166, No. 3, pp. 321–327, https://doi.org/10.1680/geng.10.00029

McNabb, D. H. and Boersma, L., 1996, "Nonlinear Model for Compressibility of Partly Saturated Soils," *Soil Sci. Soc. Am. J.*, Vol. 60, No. 2, pp. 333–341, https://doi.org/10.2136/sssaj1996.03615995006000020003x

Moayed, R. Z., Kordnaeij, A., and Mola-Abasi, H., 2016, "Compressibility Indices of Saturated Clays by Group Method of Data Handling and Genetic Algorithms," *Neural Comput. Appl.*, pp. 1–14, https://doi.org/10.1007/s00521-016-2390-9

Nagaraj, H. B., Munnas, M., and Sridharan, A., 2010, "Swelling Behavior of Expansive Soils," *Int. J. Geotech. Eng.*, Vol. 4, No. 1, pp. 99–110, https://doi.org/10.3328/ijge.2010.04.01.99-110

Nalbantoglu, Z. and Tuncer, E. R., 2001, "Compressibility and Hydraulic Conductivity of a Chemically Treated Expansive Clay," *Can. Geotech. J.*, Vol. 38, No. 1, pp. 154–160, https://doi.org/10.1139/t00-076

Oikawa, H., 1987, "Compression Curve of Soft Soils," *Soils Found.*, Vol. 27, No. 3, pp. 99–104, https://doi.org/10.3208/sandf1972.27.3_99

Onitsuka, K., Hong, Z., Hara, Y., and Yoshitake, S., 1995, "Interpretation of Oedometer Test Data for Natural Clays," *Soils Found.*, Vol. 35, No. 3, pp. 61–70, https://doi.org/10.3208/sandf.35.61

Onyejekwe, S., Kang, X., and Ge, L., 2014, "Assessment of Empirical Equations for the Compression Index of Fine-Grained Soils in Missouri," *Bull. Eng. Geol. Environ.*, Vol. 74, No. 3, pp. 705–716, https://doi.org/10.1007/s10064-014-0659-8

Pacheco Silva, F., 1970, "A New Graphical Construction for Determination of the Preconsolidation Stress of a Soil Sample," presented at the *Fourth Brazilian Conference on Soil Mechanics and Foundation Engineering*, Rio de Janeiro, Brazil, International Society for Soil Mechanics and Geotechnical Engineering, London, England, pp. 225–232.

Pestana, J. M. and Whittle, A. J., 1995, "Compression Model for Cohesionless Soils," *Géotechnique*, Vol. 45, No. 4, pp. 611–631, https://doi.org/10.1680/geot.1995.45.4.611

Sivapullaiah, P. V., Sridharan, A., and Stalin, V. K., 1996, "Swelling Behaviour of Soil-Bentonite Mixtures," *Can. Geotech. J.*, Vol. 33, No. 5, pp. 808–814, https://doi.org/10.1139/t96-106-326

Soltani, A., 2016, "Discussion of 'Compressibility Behavior of Soils: A Statistical Approach' by Syed Iftekhar Ahmed and Sumi Siddiqua, Geotechnical and Geological Engineering, Vol. 34, No. 6, [doi: 10.1007/s10706-016-9996-7]," *Geotech. Geol. Eng.*, Vol. 34, No. 5, pp. 1687–1692, https://doi.org/10.1007/s10706-016-0062-2

Sridharan, A., Abraham, B. M., and Jose, B. T., 1991, "Improved Technique for Estimation of Preconsolidation Pressure," *Géotechnique*, Vol. 41, No. 2, pp. 263–268, https://doi.org/10.1680/geot.1991.41.2.263

Sridharan, A. and Allam, M. M., 1982, "Volume Change Behavior of Desiccated Soils," *J. Geotech. Eng. Div.*, Vol. 108, No. 8, pp. 1057–1071, https://doi.org/10.1016/0148-9062(83)91686-8

Sridharan, A. and Gurtug, Y., 2005, "Compressibility Characteristics of Soils," *Geotech. Geol. Eng.*, Vol. 23, No. 5, pp. 615–634, https://doi.org/10.1007/s10706-004-9112-2

Sridharan, A. and Gurtug, Y., 2004, "Swelling Behaviour of Compacted Fine-Grained Soils," *Eng. Geol.*, Vol. 72, Nos. 1–2, pp. 9–18, https://doi.org/10.1016/S0013-7952(03)00161-3

Sridharan, A., Rao, A., and Sivapullaiah, P., 1986a, "Swelling Pressure of Clays," *Geotech. Test. J.*, Vol. 9, No. 1, pp. 24–33, https://doi.org/10.1520/GTJ10608J

Sridharan, A., Rao, S. M., and Murthy, N. S., 1986b, "Compressibility Behaviour of Homoionized Bentonites," *Géotechnique*, Vol. 36, No. 4, pp. 551–564, https://doi.org/10.1680/geot.1986.36.4.551

Sridharan, A. and Sreepada Rao, A., 1981, "Rectangular Hyperbola Fitting Method for One-Dimensional Consolidation," *Geotech. Test. J.*, Vol. 4, No. 4, pp. 161–168, https://doi.org/10.1520/GTJ10785J

Sridharan, A. and Venkatappa Rao, G., 1973, "Mechanisms Controlling Volume Change of Saturated Clays and the Role of the Effective Stress Concept," *Géotechnique*, Vol. 23, No. 3, pp. 359–382, https://doi.org/10.1680/geot.1973.23.3.359

Stark, T. D., Ebeling, R. M., and Vettel, J. J., 1994, "Hyperbolic Stress-Strain Parameters for Silts," *J. Geotech. Eng.*, Vol. 120, No. 2, pp. 420–441, https://doi.org/10.1061/(ASCE)0733-9410(1994)120:2(4200029

Subba Rao, K. S. and Tripathy, S., 2003, "Effect of Aging on Swelling and Swell-Shrink Behaviour of a Compacted Expansive Soil," *Geotech. Test. J.*, Vol. 26, No. 1, pp. 36–46, https://doi.org/10.1520/gtj11100j

Viswanadham, B. V. S., Phanikumar, B. R., and Mukherjee, R. V., 2009, "Swelling Behaviour of a Geofiber-Reinforced Expansive Soil," *Geotext. Geomembranes*, Vol. 27, No. 1, pp. 73–76, https://doi.org/10.1016/j.geotexmem.2008.06.002